evapotranspiration following changes in climate and vegetation cover during an ecological restoration period (2000–2015) in the Loess Plateau, China. *Science of the Total Environment*, **689**, 534-545, 1 November 2019.

Mahmood, R. & Jia, S. (2019). Assessment of hydro-climatic trends and causes of dramatically declining stream flow to Lake Chad, Africa, using a hydrological approach. *Science of the Total Environment*, **675**, 122-140, 20 July 2019.

Mallucci, S., Majone, B., & Bellin, A. (2019). Detection and attribution of hydrological changes in a large Alpine river basin. *J. Hydrology*, **575**, 1214-1229, August 2019.

Markovich, K.H., Dahlke, H.E., Arumí, J.L., Maxwell, R.M., & Fogg, G.E. (2019). Bayesian hydrograph separation in a minimally gauged alpine volcanic watershed in central Chile. *Hydrology*, **575**, 1288-1300, August 2019.

Mavis, F.T. & L.M. Lauschey (1948). "A Reappraisal of the beginning of bed-movement-competent
velocity, "*International Association for Hydraulic Research, Second Meeting*, Stockholm, June 1948.

McGregor, G.R. (2019). "Climate and rivers." *River Research and Applications*, 1-22, https://doi.org/10.1002/rra.3508

N.A.S.A. (2017). "Earth Observatory", National Aeronautics and Space Administration, <https://earthobservatory.nasa.gov/IOTD/view.php?id=83624>, accessed August 2017.

Nguvava, M., Abiodun, B., & Otieno, F. (2019). Projecting drought characteristics over East African basins at specific global warming levels. *Atmospheric Research*, **228**, 41-54, 1 November 2019.

Nilawar, A. P., & Waikar, M. L. (2019). Impacts of climate change on streamflow and sediment concentration under RCP 4.5 and 8.5: A case study in Purna river basin, India. *Science of the Total Environment*, **650**, 2685– 2696. https://doi.org/10.1016/j.scitotenv.2018.09.334

Novoa, V., Ahumada-Rudolph, R., Rojas, O., Sáez, K., de la Barrera, F., & Arumí, J.L. (2019). Understanding agricultural water footprint variability to improve water management in Chile. *Science of the Total Environment*, **670**, 188-199, 20 June 2019.

O'Briain, R. (2019). Climate change and European rivers: An eco-hydromorphological perspective. *Ecohydrology*, **12**(5), July 2019.

Piniewski, M. (2017). Classification of natural flow regimes in Poland. *River Research and Applications*, **33**(7), https://doi.org/10.1002/rra.3153.

Piniewski, M., Laizé, C.L.R., Acreman, M.C., Okruszko, T., & Schneider, C. (2014). Effect of climate change on environmental flow indicators in the Narew Basin, Poland. *J. Environmental Quality*, **43(**1), 155-167, January/February 2014.

Rubey, W.W. (1933). "Settling velocities of gravel, sand, and silt particles." *American Journal of Science*, **25**, 325-338.

Saifullah, M., Liu, S., Tahir, A.A., Zaman, M., Ahmad, S., Adnan, M. Chen, D., Ashraf, M., & Mehmood, A. (2019). Development of threshold levels and a climate-sensitivity model of the hydrological regime of the high-altitude catchment of the Western Himalayas, Pakistan. *Water* (Switzerland), **11**(7), July 1, 2019.

Shen, H.W. & Hung, C.S. (1972). "An Engineering Approach to Total Bed Material Load by Regression Analysis." *Proc. Sedimentation Symp.,* 14-11 to 14-17.

Shrestha, B., Maskey, S., Babel, M. S., van Griensven, A., & Uhlenbrook, S. (2018). Sediment related impacts of climate change and reservoir development in the Lower Mekong River Basin: A case study of the Nam Ou Basin, Lao PDR. *Climatic Change*, **149**, 13– 27.

Strickler, A. (1923). “Beiträzo zur Frage der Gerschwindigheits formel und der Rauhigkeitszahlen für Strome Kanale und Geschlossene Leitungen,” *Mitteilungen des Eidgenossischer Amtes f*ür *Wasserwirtschaft, Bern.*

Wang, Y., Luo, Y., & Shafeeque, M. (2019). Interpretation of vegetation phenology changes using daytime and night-time temperatures across the Yellow River Basin, China. *Science of the Total Environment*, **693**(25) November 2019.

White, F.M., (1999) “Fluid Mechanics.” Mc-Graw Hill, Boston, Mass.

Whitehead, P.G., Jin, L., Bussi, G., Voepel, H.E., Darby, S.E., Vasilopoulos, G., Manley, R., Rodda, H., Hutton, C., Hackney, C., Tri, V.P.D., & Hung, N.N. (2019). Water quality modelling of the Mekong River basin: Climate change and socioeconomics drive flow and nutrient flux changes to the Mekong Delta. *Science of the Total Environment*, **673**, 218-229, 10 July 2019.

Yang, X., Yu, X., Wang, Y., Liu, Y., Zhang, M., Ren, L., Yuan, F., & Jiang, S. (2019). Estimating the response of hydrological regimes to future projections of precipitation and temperature over the upper Yangtze River. *Atmospheric Research*, **230**(1) December 2019.

Yilmaz, Y.A. Sen, O.L., & Turuncoglu, U.U. (2019). Modeling the hydroclimatic effects of local land use and land cover changes on the water budget in the upper Euphrates – Tigris basin. *J. Hydrology*, **576**, 596-609, September 2019.

Zhang, Y., Wang, Y., Chen, Y., Liang, F., & Liu, H. (2019). Assessment of future flash flood inundations in coastal regions under climate change scenarios—A case study of Hadahe River basin in northeastern China. *Science of the Total Environment*, **693**(25) November 2019.

Simulation of Shoreline Changes on the Delaware Coast near the Indian River Inlet

Yan Ding[1]; Sung-Chan Kim[2]; Rusty Permenter[3]; Richard Styles[4]; and Jeffrey A. Gebert[5]

[1]U.S. Army Engineer Research and Development Center, Coastal and Hydraulics Laboratory, Vicksburg, MS, USA
[2]U.S. Army Engineer Research and Development Center, Coastal and Hydraulics Laboratory, Vicksburg, MS, USA
[3]U.S. Army Engineer Research and Development Center, Coastal and Hydraulics Laboratory, Vicksburg, MS, USA
[4]U.S. Army Engineer Research and Development Center, Coastal and Hydraulics Laboratory, Vicksburg, MS, USA
[5]U.S. Army Corps of Engineers, Philadelphia District, Philadelphia, PA, USA

ABSTRACT

The purpose of this study is to model long-term shoreline changes on the Delaware coast near the Indian River Inlet (IRI) by using the U.S. Army Corps of Engineers shoreline evolution model, GenCade. By utilizing shoreline survey data and bathymetrical data of the inlet, this site-specific model was validated by hindcasting a 12-year-long historical shoreline evolution. The corresponding coastal processes simulated in the model include inlet sediment transport, offshore waves, longshore sediment transport, and coastal protection practices such as sand bypassing operation and beach nourishment. The evolution of shoals and bars around the inlet was simulated by using the inlet reservoir model (IRM). Model simulation skill was evaluated in terms of statistical errors by comparing simulated shoreline changes with observation data. The effect of sand bypassing operation is examined by comparing simulated shoreline changes with and without the bypassing.

INTRODUCTION

Along Delaware's Atlantic coast, an approximately 24 mile long, straight coast, long-term average shoreline configurations are largely determined by antecedent geology and inlet morphology, while variations of shoreline are influenced by seasonal changes of waves, episodic events (e.g. tropical storms and hurricanes), and coastal protection practices (e.g. structure installation, mechanical sand bypassing, beach nourishment). The Indian River Inlet is located almost at the mid-point of the coast and connects the Atlantic Ocean to inland bays (Figure 1). Since the 1940s, development of the Indian River Inlet for navigation purposes has significantly changed the shorelines to the north and the south, as well as evolution of shoals in the shallow water. The two constructed jetties intercept a great amount of northerly longshore sediment transport causing downdrift erosion at the north shore of IRI. Erosion protection practices such as beach fill/nourishment and sand bypassing have been applied along the coast to stabilize shoreline positions.

For mechanical sand bypassing from the updrift beach (i.e. the south shore) to the downdrift side (the north shore) of IRI, the sand bypassing system was constructed in late 1989 and started pumping operation in early 1990 (Clausner et al., 1992). The design bypassing rate is 84,100 m^3/year (or 110,000 cubic yard (CY) per year), but the actual operational transport rate was much less than the required rate (Keshtpoor et al., 2013). Using the beach profile survey data between 1985 and 2008, Keshtpoor et al. (2013) found that before bypassing operation, the shoreline to the north of IRI retreated 10 to 60m while the south shoreline advanced up to 30m. During the bypassing operation period (1990-2010), the downdrift shoreline accreted about 10-20m relative to 1990. A gradually decreasing accretion was found within a one-mile-long north shore. Meanwhile, on the south shore (updrift beach), the beach survey data shows little variability adjacent to the inlet with retreating farther south.

Figure 1 Study area of the Delaware Coast near the Indian River Inlet, a crane-mounted eductor for pumping sand in the south shore, and the beach for post-storm nourishment (May-Nov. 2013)

Before the sand bypassing system became operational, the north shore was occasionally nourished by using the sand sources in the back bay and flood shoals. Keshtpoor et al. (2013) reported eight beach fill efforts between 1957 and 1990 with a range of volume from 137,620 to 591,770 m^3. Recently, a 403,570 m^3 post-storm rehabilitation beach nourishment was conducted along the northern shore of IRI from May to October 2013. (Gebert, 2018).

The Indian River Inlet navigation and sandy bypass project has been a focus of many studies for sand bypassing, dredging, beach nourishment (e.g. Keshtpoor et al., 2013; USACE-NAP, 2018). Delaware kept records of the history of state-led beach fills since the 1950s and federal beach fill projects since 2004. Beach profiles and nearshore waves are two critical variables for predicting shoreline evolutions. Regular transects of the Delaware shoreline exist from 2004 with wave observation data from USACE at Bethany, Dewey, and Ocean City (USACE 1996). Valuable studies on longshore sediment transport (LST) were done by Puleo (2010) by using Wave Information Studies wave buoy data (WIS, 2019) and the US Army Corps of Engineers' Coastal Engineering Research Center (CERC) longshore sediment transport formulation. It was found that the 20-year mean LST rate varies from 470,970 to 517,070 m^3/year. But more factors due to shoreline evolution, beach refilling/sand bypassing projects, longshore sediment transport, sea level rise, etc. need to be investigated.

The main purpose of the study is to apply the shoreline evolution model, GenCade to reproduce the historical shoreline evolution along the Delaware coast around the Indian River Inlet. The model takes into account environmental factors such as inlet sediment transport, offshore waves, and longshore sediment transport, as well as erosion protection practices like beach nourishment and sand bypassing process at the study site. The inlet reservoir model in

GenCade is examined by simulating sediment transport processes across the Indian River Inlet and the evolution of shoal and bar volumes. Sand bypassing capability of the inlet elements systems is quantified by using a newly-defined sediment transport factor to measure the transfer rate of longshore sediment through an inlet from updrift side to the downdrift. Model simulation skill is assessed by comparing simulated shoreline changes with observation data. The effect of sand bypassing operation is evaluated by comparing the shoreline changes with and without the bypassing.

GENCADE AND INLET RESERVOIR MODEL

GenCade (Frey et al., 2012) is a USACE general engineering application tool to simulate long-term shoreline changes on coasts with structures, beach fills, inlets, and various boundary conditions. The model calculates longshore sediment transport rates (i.e. CERC formula) induced by waves and tidal currents, shoreline change, tidal inlet shoal and bar volume evolution, natural bypassing, and the fate of coastal restoration and stabilization projects. It has been widely used in coastal engineering projects for shoreline erosion protection, coastal sediment management, and coastal hazard management (e.g. Hanson et al., 2011; Milligan & Hardaway, 2014; Frey, 2015). Recent development and validation of the model has provided new simulation capabilities including cross-shore sediment transport processes, sea level rise, and subsidence, as well as probabilistic shoreline change prediction (e.g. Ding et al., 2018, 2019a,b). Cross-shore sediment transport plays an important role in driving beach evolution including shoreline movement and bar migration. A semi-empirical model for estimating the phase-averaged net cross-shore transport rate has been implemented into GenCade and was validated by simulating shoreline changes at a barred beach (Ding et al., 2019a, b). The capabilities and processes for cross-shore sediment transport and the Monte-Carlo simulation are recently developed. One may refer to Ding et al. (2018) and (2019a) for the details of those new simulation capabilities.

Kraus (2000) and Larson et al. (2003, 2006) developed the Inlet Reservoir Model (IRM) and implemented into GenCade to simulate sediment bypassing (transport) from the updrift barrier to the downdrift barrier and between flood and ebb shoals, based on an equilibrium assumption of shoal volumes. Figure 2 illustrates six morphological elements, i.e. flood and ebb shoals, a bypass bar and an attachment bar in each side of the inlet, as well as an inlet channel. We keep the same mathematical expressions as Frey et al. (2012) to define sand volume of each morphological element and sediment flux passing from one element to another. For example, given that V_x is a sand volume of a morphological element (shoal or bar), then V_{xq} represents an equilibrium volume of this element. The subscript x is a placeholder for subscripts a (attachment bars), b (bypass bars), e (ebb shoal), or f (flood shoal). Each morphological element is assumed to have a certain equilibrium volume for fixed hydrodynamic and sediment conditions. Starting from the updrift side, the IRM proportionally distributes the updrift alongshore sediment transport flux Q_{in} to the two immediate downdrift elements, ebb and flood shoals, then bypass bar, attachment bar, and to the downdrift beach. The received sand transport at the downdrift side Q_{out} is dependent on the volume changes of all the inlet morphological elements. By assembling the equations of the transport fluxes (page 38 in Frey et al., 2012), one equation as a direct relationship between the updrift sediment flux Q_{in} and the received downdrift Q_{out} is derived as follows:

$$Q_{out} = \begin{cases} \frac{V_e}{V_{eq}}\frac{V_b}{V_{bq}}\frac{V_a}{V_{aq}}\left[(\delta+\beta(1-\delta))\right]Q_{in}, & V_f \le V_{fq} \\ \frac{V_e}{V_{eq}}\frac{V_b}{V_{bq}}\frac{V_a}{V_{aq}}\left[(\delta+\beta(1-\delta))+\frac{V_f-V_{fq}}{Q_{in}\Delta t}\right]Q_{in}, & V_f > V_{fq} \end{cases} \tag{1}$$

where Δt =simulation time step,

$$\delta = \frac{V_e + V_f}{V_{eq} + V_{fq}} \tag{2}$$

$$\beta = \frac{1 - V_e / V_{eq}}{2 - V_e / V_{eq} - V_f / V_{fq}} \tag{3}$$

By defining a transfer parameter γ as

$$\gamma = \begin{cases} \frac{V_e}{V_{eq}}\frac{V_b}{V_{bq}}\frac{V_a}{V_{aq}}\left[(\delta+\beta(1-\delta))\right], & V_f \le V_{fq} \\ \frac{V_e}{V_{eq}}\frac{V_b}{V_{bq}}\frac{V_a}{V_{aq}}\left[(\delta+\beta(1-\delta))+\frac{V_f-V_{fq}}{Q_{in}\Delta t}\right], & V_f > V_{fq} \end{cases} \tag{4}$$

the downdrift flux received from the updrift side of the inlet is therefore proportional to the Q_{in}, i.e.

$$Q_{out} = \gamma Q_{in} \tag{5}$$

This time-dependent transfer parameter is a function of the actual and equilibrium volumes of six morphological elements (two shoals, two bypassing bars, and two attachment bars), which are 12 model (empirical) parameters in the IRM model. The other equations for calculating actual volume changes in shoals and bars can be found in Kraus (2000) and Frey et al. (2012).

Based on the above-mentioned equations on sediment bypassing processes, the IRM model enables to simulate sediment exchanges between the inlet morphological elements and the evolution of the elements' volumes. However, configuration of an IRM model through calibrating all the 12 empirical parameters for actual and equilibrium volumes is a challenge task, and relies on field data of morphological changes near inlet.

GENCADE MODEL CONFIGURATION AND SHORELINE SURVEY DATA

The GenCade model was developed to simulate shoreline evolution on the coasts near the IRI for a 12-year-long period from 2005/03/12 0:00 to 2016/12/31 0:00. As shown in Figure 1, the simulated coastline is 10-km long, centered around the inlet, with a grid size of 25 m. A NAVD88-based zero contour line calculated from a LIDAR dataset in 2005 was used as the initial shoreline. Based on the survey data, it has been estimated that the sediment closure depth is approximately 10.0 m, and the berm height is 2.0 m. The boundary condition of fixed shoreline position is given at the two ends of the shoreline, almost 5 km away from the inlet, where are far enough not to impact shoreline changes at the inlet. The sediment grain size for calculating the sediment transport rate was set to 0.3 mm, a typical value in a cross-shore profile. To calculate the longshore sediment transport rate, the two empirical parameters of CERC formulation, K_1 and K_2 , need to be determined. Based on the suggested values by Larson et al. (2006), we calibrated the two parameters in the present simulation, and found that K_1 is set to 0.17 on the north shore, and 0.35 on the south shore; K_2 is 0.085 on the north and 0.175 on the south. For this simulation, the calculation of cross-shore sediment transport is excluded. For the sand bypassing operation, we used the annual bypassing rate (61,300 m^3/year) obtained by means of the least squares regression by Keshtpoor et al. (2013). This bypassing rate is less than the designed value (i.e. 84,100 m^3/year). Moreover, a 403,570 m^3 post-storm rehabilitation beach nourishment during the period from May to October 2013 was also included in the simulation

(Gebert, 2018).

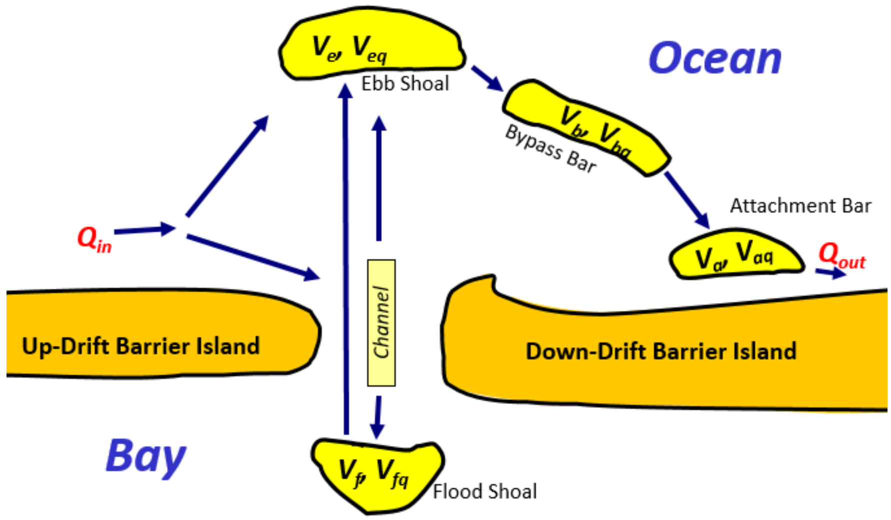

Figure 2 Sediment bypassing and evolution of shoals in the Inlet Reservoir Model

The offshore wave parameters (significant wave height, period, and mean direction) are given by observation data at two WIS wave buoys, Station ID 63156 (20-m depth offshore) and 63158 (18-m depth) (WIS, 2019). Over the 12-year simulation period, the average significant wave height is approximately 1.0 m, and the mean wave direction is SSE. This causes a predominant northward longshore sediment transport.

The Delaware coastlines are monitored by the Delaware Department of Natural Resources and Environmental Control (DNREC) and USACE Philadelphia District (NAP). The data set of the Line Reference Points (LRP) covers the whole length of Delaware coastlines though sparsely over 10 year period since 2004. This data set has highly varying profiles around zero elevation so that it would be difficult to determine shorelines by extracting zero elevations. On the coasts near the IRI during the simulation period (2005 – 2017), DNREC has reported beach profile survey data, eight profile lines on the north and south beaches (16 lines total). The monitoring survey area thus includes a zone of 10,000 feet long in the longshore direction, and ~ 5,000 feet wide in the cross-shore direction. The observed shoreline positions were obtained by extracting the positions at the vertical datum (NAVD 88) from the survey data of beach profiles. A total of 218 shoreline positions were extracted from the beach profiles surveyed between June 2006 and October 2017, in which 128 valid shoreline data are located along the north shore while only 90 profiles are along the south beach.

MODEL VALIDATION RESULTS

Model validation was done by comparing the simulated shoreline positions with the observations. The statistical errors such as the root-mean-square-error (RMSE) and the coefficient of determination (R^2) are calculated to evaluate the GenCade model simulation performance. Figure 3 presents six examples for comparison of shoreline position profiles between simulation and observations: (a) 15-Jun-2008, (b) 15-Jun-2011, (c) 15-July-2012, (d) 15-Nov-2013, (e) 15-May-2014, and (f) 15-Jun-2015. The values of RMSE and R^2 for each survey time are included on each figure. The RMSE varies from 17.2 m on 15-May-2012 to 47.0

m on 15-Jun-2015. Except (f), most the R^2 values are close to unit, which means the simulated shoreline profiles match with the observed very well. Apparently, large offsets in shoreline positions can be found after 2014 (Figure 3e and 3f), which may be caused by overestimating the sand bypassing rate. Using the actual bypassing data may be needed to improve the results.

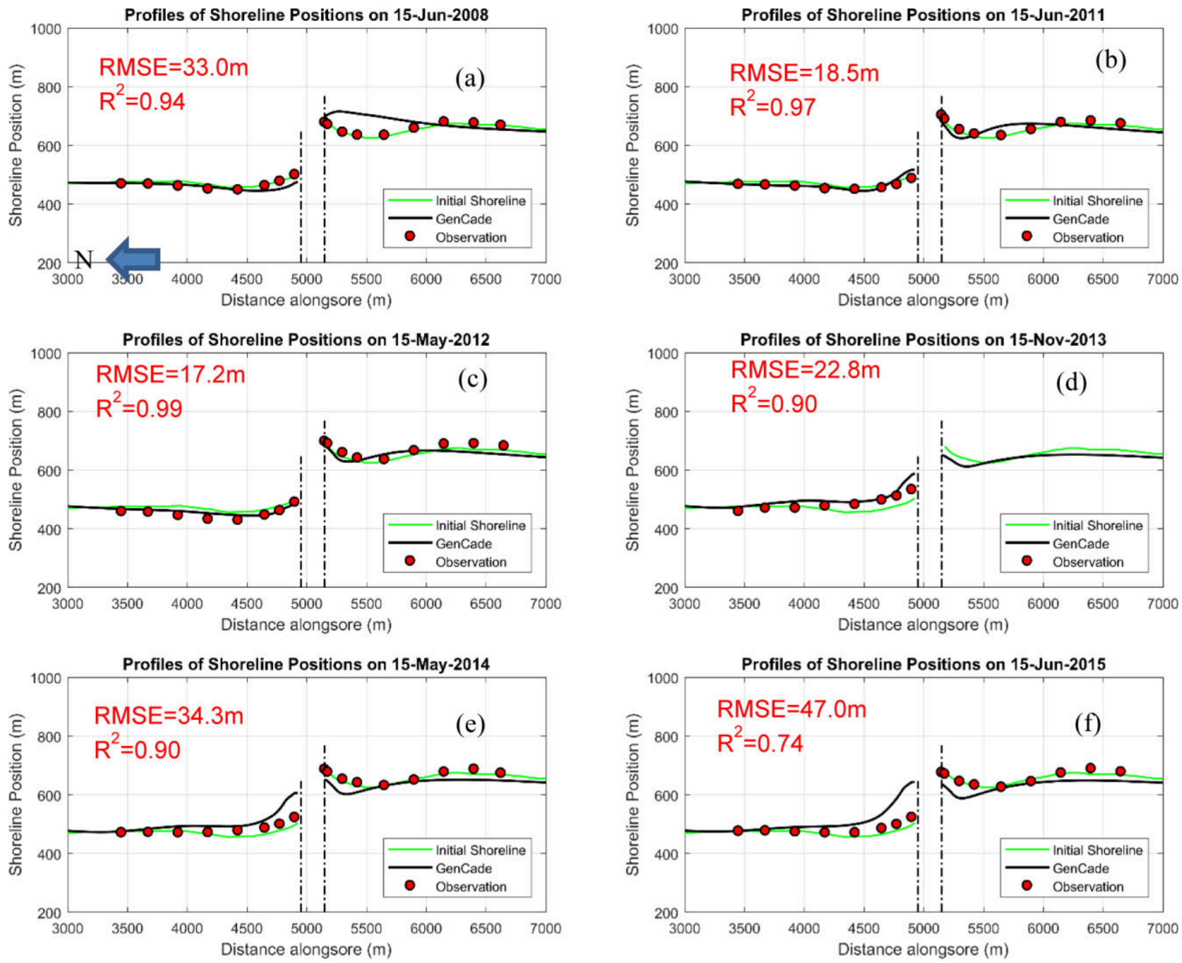

Figure 3 Comparisons of shoreline positions between observations and simulations by GenCade. The solid black lines are the simulated shoreline positions. The light green line is the initial shoreline position on 2005/03/12 0:00. The values of root-mean-square error (RMSE) and the R^2 are given on each plot. The two dash-dotted lines indicate the location of the two jetties of the IRI inlet.

As the GenCade Inlet Reservoir Model simulates the evolution of volume changes of the inlet shoals and bars (Figure 2), we can gain insight into how the model exchanges sediments around the inlet. Figure 4 presents the time histories of sand volumes at (a) flood and ebb shoal, (b) bypass bars in the north and south shores, and (3) two attachment bars in the north and south. It shows that the ebb shoal volume increases from its initial volume 4.9 Million Cubic Yard (MCY) in 2005 to 5.9 MCY in 2016, and the flood shoal slightly increases from 2.8 to 3.2 MCY over the same time period. The volumes for the two bars (bypass and attachment) on the northern shore increase slightly over the first two years and then remain the same until the end of the simulation. The model shows almost no changes in the two bars to the south. This nearly stationary state of the bars is somehow different from actual morphological changes in the area, which reflects the limits of IRM for modeling morphodynamic processes in the inlet morphological elements. Figure 4(d) presents the time history of the two sand transfer factors (γ) calculated by Eq.(4), using the sand volumes of the six inlet morphological elements. The north γ, the rate of the sand transferred from the south shore to the north, increases from 0.22 at the beginning to 0.80 after 8 years. That means about 80% of longshore sediment to the south of the inlet are being transferred to the north between 2014 to 2016. On the other side, the south γ did not change much during the entire simulation period (γ =0.12~0.15), apparently due to a lack of southward longshore sediment transport due to the predominant wave forcing. The best estimates of the initial and equilibrium volumes of two shoals and four bars are given in Table 1. Please note that the values of the volumes were calculated by the IRM, which reflects the simulated shoreline changes around the inlet. Further verification of the shoal volume changes needs to be done by using hydrographic survey data.

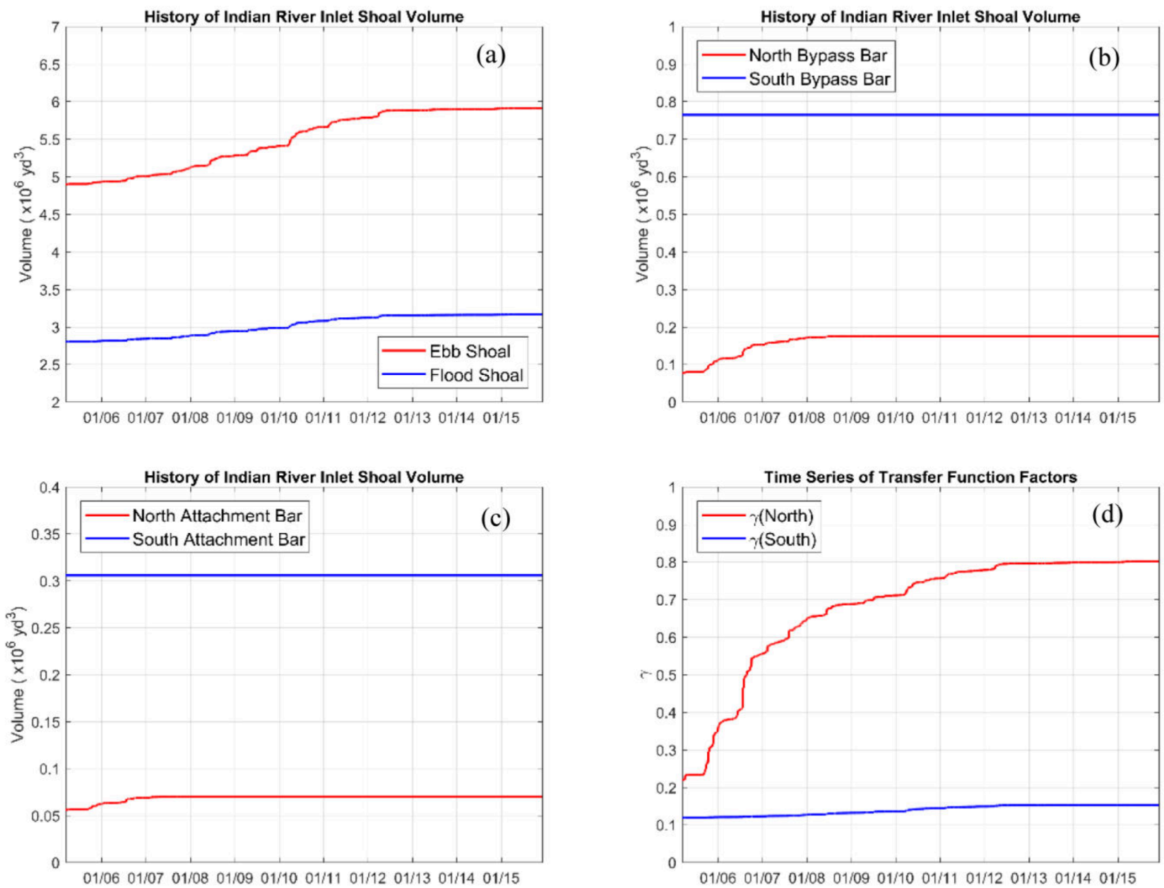

Figure 4 Evolution of inlet shoal and bars. (a) History of the volumes of flood and ebb shoals. (b) Volumes changes in the north and south bypass bar. (c) Volume changes in the attachment bars at the north and south shores. (d) History of sand transfer factors defined by Eq.(4).

To quantify the effect of the sand bypassing operation on the shoreline change, one simulation of shoreline change without sand bypassing was performed. The other calibrated GenCade model parameters remained the same. As an example, Figure 5 compares two time histories of shoreline position with and without sand bypassing at two locations near the two jetties at (a) 225-m north from the north jetty and (b) 150-m south from the south jetty. Figure 5 (c) shows the shoreline accretion in the north side driven only by the sand bypass operation; and (d) the retreat at the location of the south shore. The accretion to the north of the inlet shows that the shoreline advances approximately 10 m in the first 5 years and then almost linearly increases up to 80m at the end of 2016. The shoreline retreat to the south of the inlet due to sand borrowing was slow until 2012, and then sped up to about 30m at the end of simulation. The model correctly responds to the sand bypassing operation along the north and south shorelines; however, the bypass rate may be overestimated, which causes the exaggerated shoreline changes after 2014. Again, the actual bypassing data should be used for improving the model validation.

Table 1 Estimated initial and equilibrium volumes in inlet shoals and bars

	Initial (yd^3)*	Equilibrium (yd^3)
Ebb shoal	4,900,000	7,000,000
Flood shoal	2,800,000	3,500,000
North bypass bar	76,540	175,000
North attachment bar	56,000	70,000
South bypass bar	764,500	1,749,999
South attachment bar	305,800	700,000

*: 1 yd^3 = 0.7646m^3

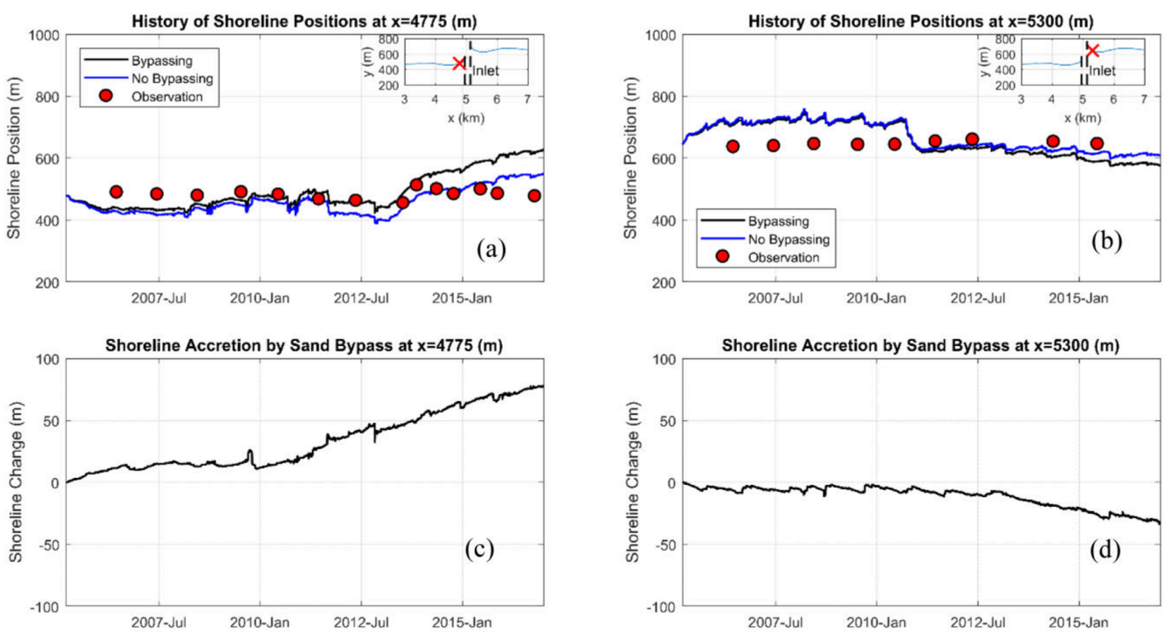

Figure 5 Comparisons of histories of shoreline position with and without sand bypassing. The observation data are for the results with the sand bypassing. (a): History of shoreline position at the north shore, 225 m from the north jetty. The symbol "X" in the box at the upper right corner shows the transect of the shoreline position. (b) History of shoreline position at the south shore, 150 m south of the south jetty. (c): History of shoreline accretion due to sand bypassing at the north shore. (d): the shoreline accretion due to sand bypassing at the south shore.